Journal of the Indian Academy of Wood Science (2026) 23:81–92
https://doi.org/10.1007/s13196-025-00397-y

ORIGINAL ARTICLE

Predicting the impact of short-duration densification on timber set-recovery using generalized additive model and transformed ordinary least squares regression

Charles Michael Albert[1] · **Kang Chiang Liew**[1]

Received: 30 May 2025 / Accepted: 17 November 2025 / Published online: 14 January 2026
© The Author(s) 2026

Abstract
This study examined the effects of varying compression ratios (40%, 50%, and 60%) applied during the short-duration densification on the set-recovery and density of laminas of *Paraserianthes falcataria*, a low-density timber species. The densification process was comprised of pressing, venting, and cooling phases. Kruskal-Wallis and Dunn tests evaluated the statistical differences in set-recovery and density between different compression ratios. Modelling approaches, such as Generalized Additive Model (GAM) and Transformed Ordinary Least Squares (TOLS) regression, were developed to predict set-recovery outcomes across a broader compression ratio range (10%–80%). The non-parametric tests revealed that increased compression ratios significantly influence set-recovery and density, with a minimal increase in set-recovery and a consistent density over time. As for the dual-modelling approaches, GAM outperformed TOLS in all the model metrics. Nevertheless, both models obtained low metrics values, which were indicative of high reliability and accuracy. The overall pattern from both models suggests that set-recovery increased as the compression ratios increased. These insights are crucial for enhancing sustainable timber production, indicating potential advancements in manufacturing high-performance, eco-friendly wood materials.

Keywords Densification · Set-recovery · Paraserianthes falcataria · Generalized additive model · Transformed ordinary least square regression

Introduction

In recent years, densification technology has been studied to improve the properties of low-density wood in response to the demand for sustainable products (Neyses 2016; Pelit et al. 2018). The wood-based industry has been facing a shortage of raw materials over the past two decades, particularly in the case of medium-heavy hardwood, which requires an extended period prior to harvesting and processing (Albert and Liew 2022a). Researchers identified the potential of densification as a strategy to optimize the utilization of wood resources, especially when applied to fast-growing wood species (Albert and Liew 2022b). Densification has been in development for over a century and continues to evolve to produce wood products with desirable properties (Tu et al. 2014). The technology has been proven to enhance the physical and mechanical properties of low-density wood, enabling it to compete with existing medium-heavy hardwood (Ran et al. 2023). Various densification methods, e.g., thermo-mechanical (TM), thermo-hydro-mechanical (THM), and viscoelastic-thermal compression (VTC), have almost similar procedures, which are differentiated by the presence of pre- and post-treatment (e.g., steaming, cooling) (Neyses 2016; Schwarzkopf et al. 2018; Wang et al. 2023; Ran et al. 2023). TM focuses on heat and pressure, THM combines thermal and moisture treatment, while VTC emphasizes thermal softening (Zhao et al. 2015; Fu et al. 2017; Srivaro et al. 2021). All of these processes improve the properties of wood. Despite the advancements in wood densification, set-recovery—a phenomenon in which densified

✉ Kang Chiang Liew
liewkc@ums.edu.my

Charles Michael Albert
cmagreat@gmail.com

[1] Universiti Malaysia Sabah, Sabah, Malaysia

wood tends to recover in thickness over time—remains a limitation in the field (Bavaneghi and Ghorbani 2015).

Set-recovery is mainly influenced by relative humidity and moisture, i.e., densified wood cells tend to recover upon exposure to moisture (Neyses et al. 2016b; Luan et al. 2022). During densification, the applied pressure and elevated temperature caused the amorphous regions of the wood to become more pliable, which led to temporary plasticization (Neyses 2016). The softening behaviour of wood polymers has long been attributed to their glass transition temperatures, where hemicellulose and lignin become more deformable within the 90–170 °C range depending on moisture content (Navi and Heger 2004; Kretschmann 2010). This viscoelastic transition explains the temperature-dependent pliability observed during densification. Primary components (e.g., lignin, cellulose, and hemicellulose) that form the wood's structure undergo reorganization, enabling the material to be reshaped and compressed, which therefore results in an increase in density and mechanical strength (Laine et al. 2016; Alinoori et al. 2020). Upon the completion of densification, the plasticized wood is cooled and dried, where the temperature begins to drop below the respective glass transition temperatures of lignin, cellulose, and hemicellulose, causing them to solidify, and densified wood retains its thickness (Gonca Düzkale et al. 2019; Albert and Liew 2022b).

However, this state is unstable because if the densified wood is exposed to moisture or humidity, it tends to recover in thickness (Neyses et al. 2016b). This phenomenon occurred due to the recovery of elastic deformation in crystalline cellulose (Bekhta et al. 2015; Neyses 2016; Zhan and Avramidis 2018). In reality, densified wood did not recover to the initial thickness, but it will influence its properties, i.e., thickness recovery caused the reduction in density and mechanical strength (Laine et al. 2016). A previous study on set-recovery suggested that this reduction might occur due to (1) damaged wood cells due to densification, and (2) plasticization, leading to a certain degree of internal stress relaxation in the wood (Neyses 2016; Neyses et al. 2016b). Therefore, various approaches, such as chemical modification (acetylation and formaldehydation), pre- and post-densification treatment (heat and steam), and mechanical fixation (adhesive impregnation), have been taken to overcome this issue (Budakçı et al. 2016; Laine et al. 2016).

While a large number of studies have resulted in the reduction of set-recovery, there is no approach that successfully eliminates it due to the hygroscopic nature of wood (Buchelt et al. 2014; Neyses et al. 2016a; Schwarzkopf 2021). Although the relationship between densification and set-recovery had been reported in previous studies, most of those works involved temperate hardwoods and longer pressing durations (Navi and Heger 2004; Tu et al. 2014).

The present study extended this understanding by applying a short-duration densification process to *Paraserianthes falcataria*, a fast-growing tropical species with low density. The objective of this research was to examine the influence of varying compression ratios (40%, 50%, and 60%) on the set-recovery and density of densified *Paraserianthes falcataria* laminas. Utilizing a chemical-free densification process involving three distinct short-duration phases – pressing, venting, and cooling – the study sought to identify the relationship between compression ratio and the set-recovery and density of the wood. This approach offers a deeper insight into refining densification techniques for low-density woods, contributing to the development of optimized and sustainable practices in the wood industry.

Materials and methods

Densification

Kiln-dried laminas of *Paraserianthes falcataria* (EMC: 12%) were cut into dimensions of 300 mm (l) x 50 mm (w) x 20 mm (t). This moisture level is commonly used for wood processing, as it provides adequate flexibility for deformation while preventing surface cracking or moisture-related swelling during and after pressing (Laine et al. 2016). The mean density of the laminas prior to densification was 315.09 kg/m^3. The densification was conducted using a hot-press machine with pressing temperature and pressure of 105 ± 5 °C and 6 MPa, respectively (Fig. 1). Although previous densification studies applied higher pressing temperatures (120–180 °C), a lower temperature was used in this study to prevent surface burning of the laminas. This condition also allowed partial softening of hemicellulose, which improved compressibility during the densification process while preventing severe cell rupture. The method was adapted from Albert and Liew (2025).

The total duration for the overall densification process was 900 s, which is illustrated in Fig. 2. Three compression ratios (40%, 50%, and 60%) were applied, and 30 replicates were densified for each group (Fig. 3). To achieve the targeted compression ratios, steel stoppers of specified thickness were positioned on the surface of the lower plate during hot pressing (Table 1).

The compression ratio was calculated using the method of Albert and Liew (2025) and is presented in the following equation:

$$\mathrm{CR} = \frac{\mathrm{ti\text{-}tf}}{\mathrm{ti}} \times 100 \quad (1)$$

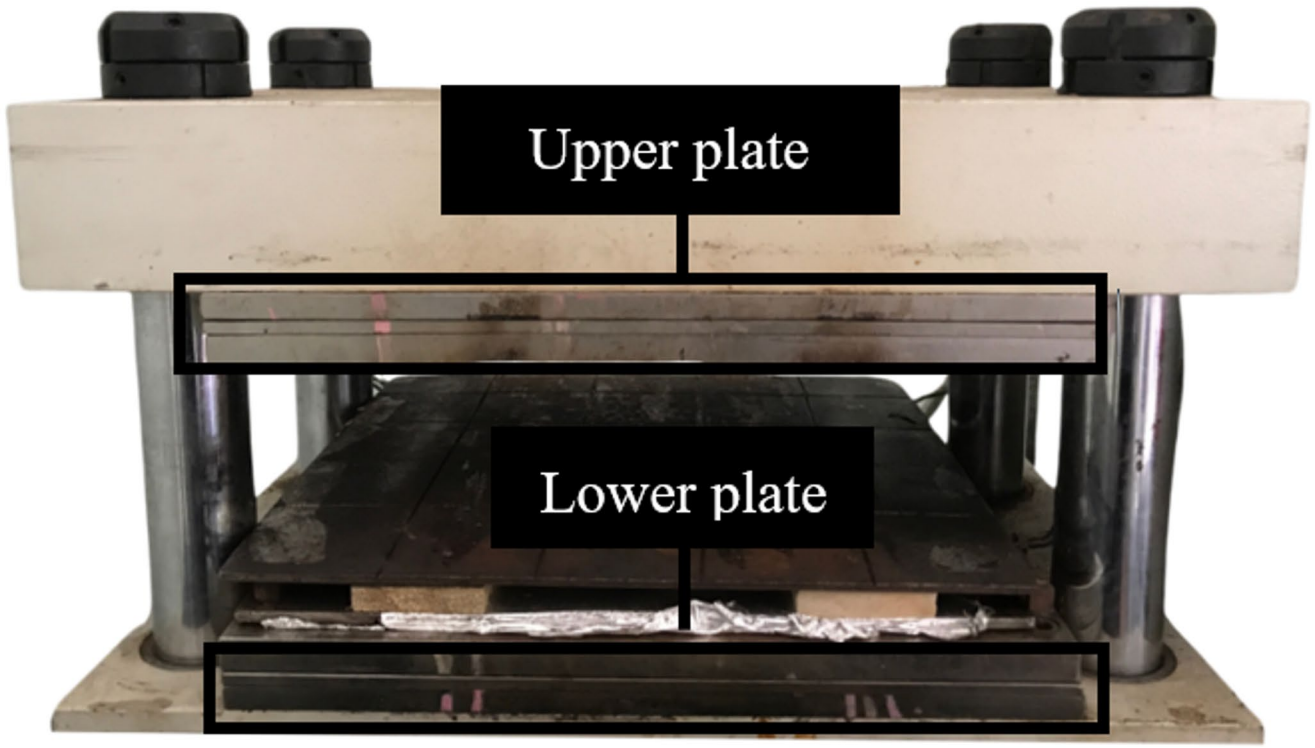


Fig. 1 Hot-press machine used for the densification

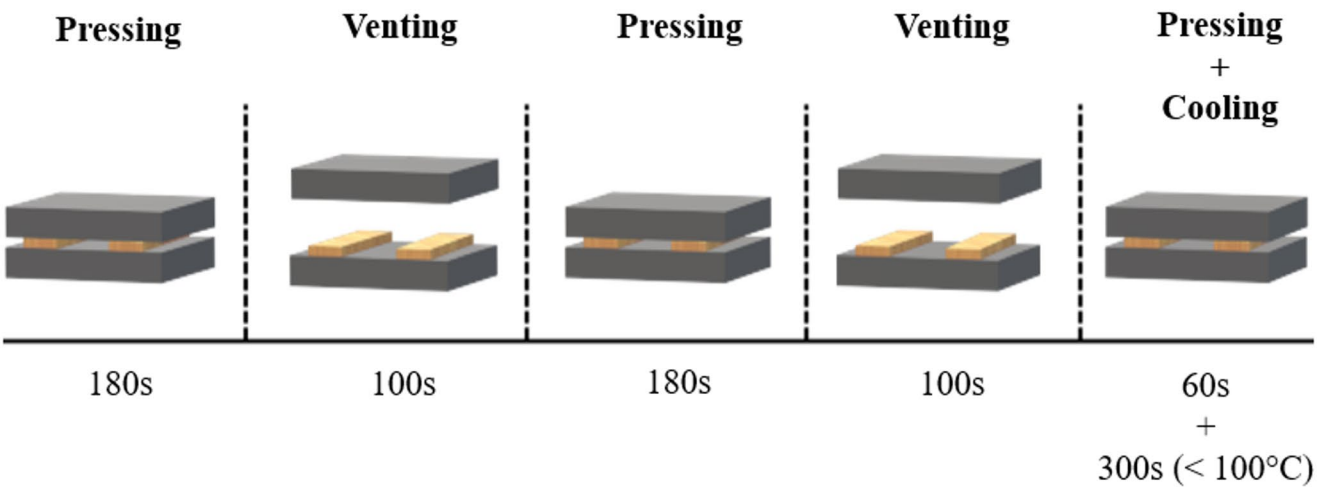


Fig. 2 Schematic visualization of distinct phases during the densification process



Fig. 3 Laminas densified at different compression ratios

Table 1 Steel stopper thickness used for each compression ratio

Compression ratio (%)	Thickness of the steel stopper (mm)
40	12
50	10
60	8

where CR is compression ratio (%), *ti* is the initial thickness (mm), and *tf* is the final thickness (mm).

The densification was initiated by pressing for 180 s and then venting for 100 s. The purpose of venting was to release moisture trapped inside the laminas, because continuous pressing without venting caused irregular shapes in the densified laminas, such as swelling and cracking (Fig. 4). The pressing and venting phases were repeated for 180 s and 100 s, respectively. After these cycles, the laminas underwent a short 60-second pressing phase, followed by a 300-second cooling phase. The cooling phase was initiated by switching off the heat and activating the water pump to circulate water through the upper and lower plates to reduce the temperature to below 100 °C. The laminas were maintained under pressure during cooling to minimise set recovery. At this temperature, hemicellulose and lignin transitioned below their glass transition temperature and began to resolidify while pressure was maintained (Neyses 2016). This re-solidification under compression stabilised the deformed cell structure and limited elastic rebound when

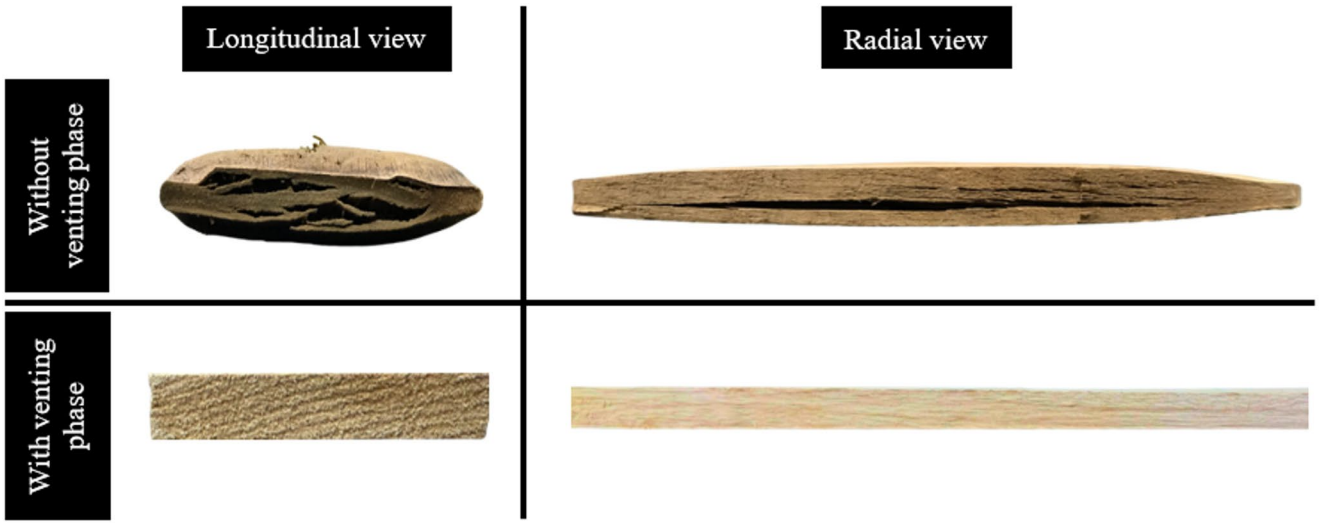


Fig. 4 Comparison of laminas densified without and with the venting phase

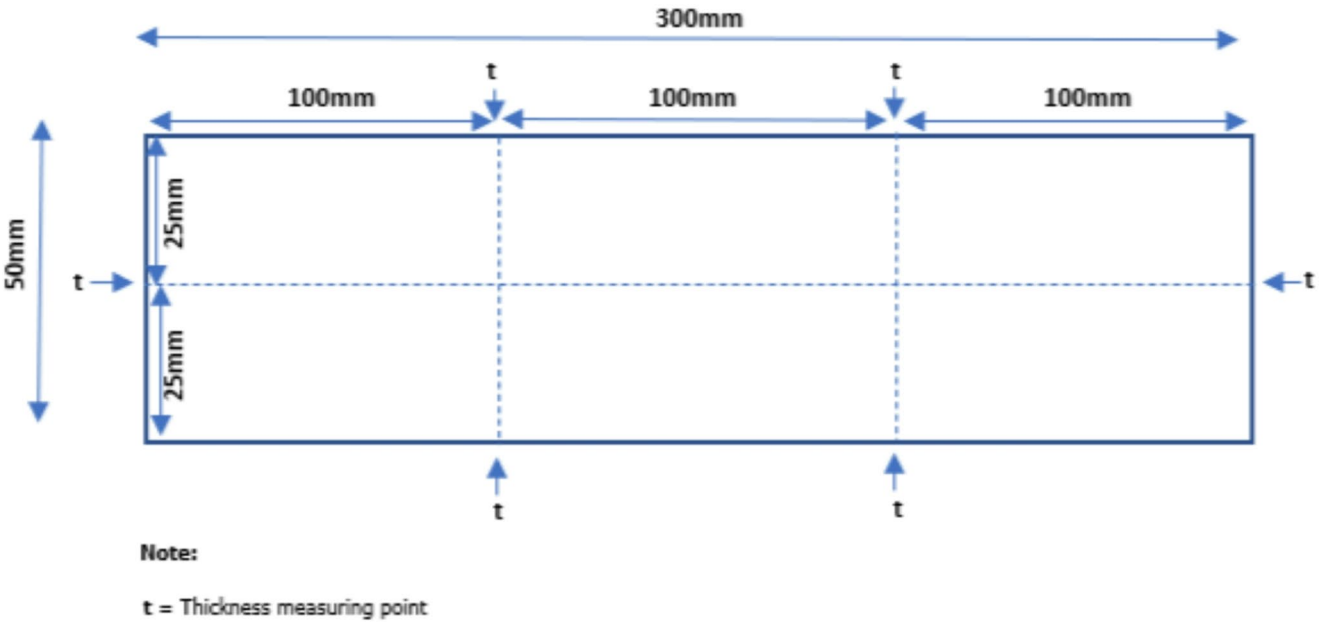


Fig. 5 Thickness measurement points for the set-recovery observation

later exposed to moisture (Neyses 2016). Upon the completion of the densification, the densified laminas were conditioned at a room temperature of 25 °C and relative humidity of 65%. Prior to further observation, the laminas achieved an average moisture content of 10–11%.

Set-recovery observation

The observation of set-recovery was performed through calipers measurement. Following conditioning, the thickness of the densified laminas was measured, by referring to guideline in Fig. 5. The set-recovery of 30 replicates from each compression ratio were measured. This procedure was repeated at 24-hour intervals and continued until the seventh day.

The thickness of the current measurement and that of the measurement taken 24 h earlier were used to calculate set-recovery, as described by Albert (2022):

$$\mathrm{SR} = \frac{\mathrm{tf} - ti}{\mathrm{tf}} \times 100 \tag{2}$$

where SR is the set-recovery (%), *tf* is the final thickness (mm), and *ti* is the initial thickness (mm).

Density observation

The density of the densified laminas was also observed at 24-hour intervals and continued until the seventh day using gravimetric method. A total of 30 replicates were measured from each compression ratio. The density was measured by referring to Albert (2022):

$$\text{Density } (\mathrm{kg/m^2}) = \frac{\text{Mass (kg)}}{\text{Volume}} \ (\mathrm{m^2}) \tag{3}$$

Statistical analyses and modelling approach

The statistical analyses and modelling were executed using R (Version 4.3.1). Preliminary assessment of the data distribution via Shapiro-Wilk tests indicated non-normality across the data sets. Therefore, non-parametric tests such as the Kruskal-Wallis test were performed to assess the effects of different compression ratios on the set recovery and density, while post-hoc test (Dunn test) was performed to find multiple comparison between groups. Furthermore, two modelling approaches, Generalized Additive Model (GAM) and Transformed Ordinary Least Square (TOLS) regression were performed to investigate the relationship between compression ratio and set-recovery, with density as the additional predictor. This dual-model approach allowed for a comprehensive understanding of the relationships between those variables. The GAM was specifically

Table 2 Mean values of set-recovery and density of laminas densified with different compression ratios

Day	Compression ratio (%)	Set Recovery (%)					Density (kg/m³)				
		df	Mean	SD	Chi-sq	*p*-value	df	Mean	SD	Chi-sq	*p*-value
1	40	2	1.29[a]	0.39	45.64	<0.0001	2	512.87[a]	64.39	49.23	<0.0001*
	50		2.40[b]	0.50				614.70[b]	59.14		
	60		3.02[b]	1.48				689.62[c]	80.13		
2	40	2	0.96[a]	0.25	66.58	<0.0001	2	509.20[a]	64.00	45.34	<0.0001*
	50		0.63[b]	0.24				601.98[b]	56.60		
	60		2.03[c]	0.34				671.17[c]	78.02		
3	40	2	0.28[a]	0.15	62.15	<0.0001	2	508.67[a]	64.04	44.00	<0.0001*
	50		0.45[a]	0.19				600.32[b]	56.48		
	60		1.16[b]	0.34				665.71[c]	77.49		
4	40	2	0.18[a]	0.07	55.24	<0.0001	2	507.76[a]	63.98	43.82	<0.0001*
	50		0.22[a]	0.08				599.21[b]	56.45		
	60		0.53[b]	0.17				663.80[c]	77.36		
5	40	2	0.10[a]	0.03	39.22	<0.0001	2	507.23[a]	63.88	43.71	<0.0001*
	50		0.21[b]	0.09				597.97[b]	56.31		
	60		0.23[b]	0.08				663.25[c]	77.44		
6	40	2	0.07[a]	0.03	30.69	<0.0001	2	506.87[a]	63.79	43.40	<0.0001*
	50		0.12[b]	0.05				597.24[b]	56.32		
	60		0.15[b]	0.07				662.37[c]	77.39		
7	40	2	0.07[a]	0.04	2.61	0.2717	2	506.50[a]	63.73	43.77	<0.0001*
	50		0.09[a]	0.06				596.68[b]	56.22		
	60		0.09[a]	0.04				661.76[c]	77.25		

Different superscripts [abc] indicate a significant difference among the compression ratios (p value < 0.05)

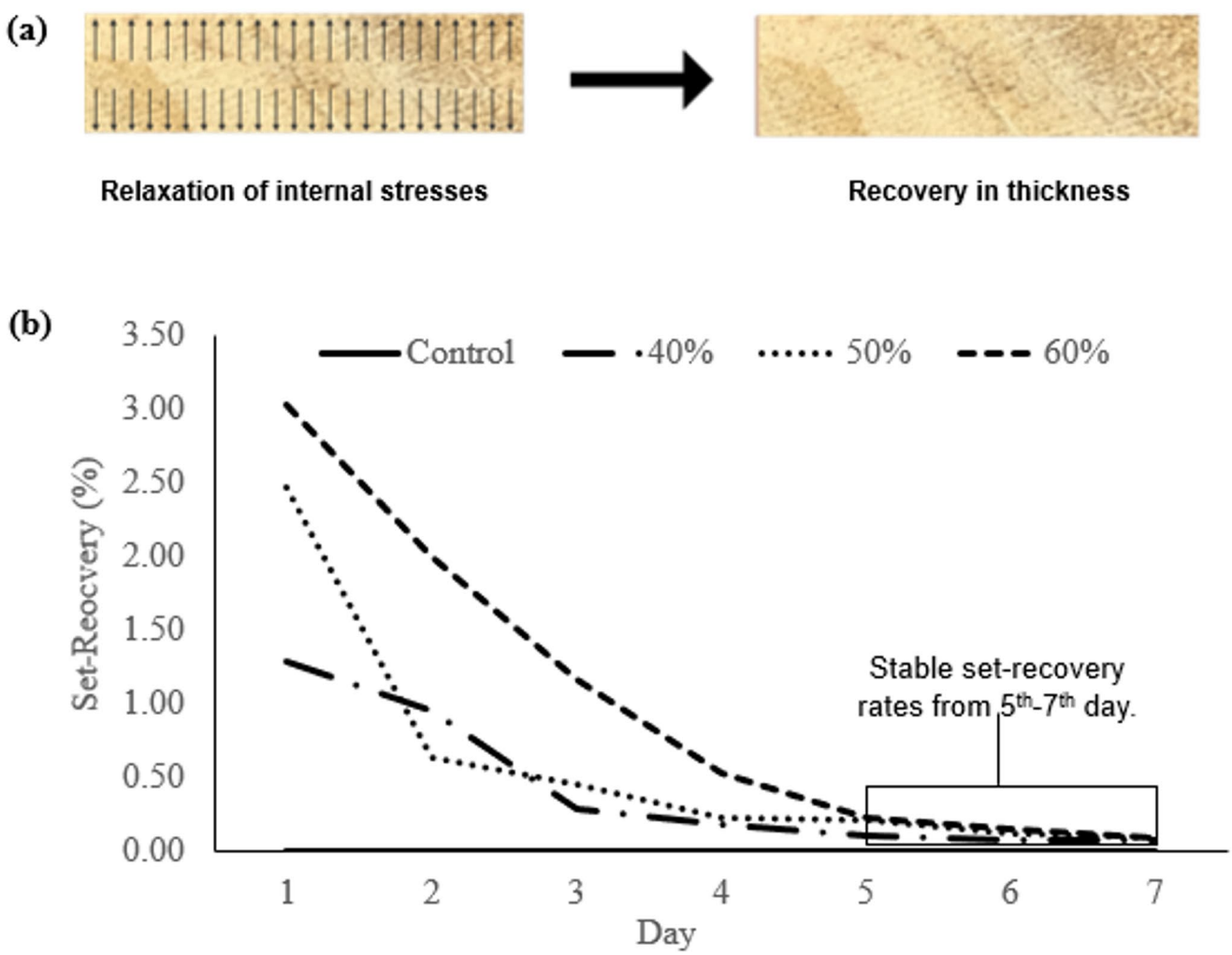


Fig. 6 Set-recovery: **a** schematic visualization of set-recovery during post-densification; **b** seven days set-recovery (mean values) observation for the densified laminas

useful in capturing the non-linear relationship and interactions between compression ratios, density and set-recovery (Cuny et al. 2013). The GAM is computed as:

$$\mathrm{SR} = \beta 0 + f1(CR) + f2(D) + \epsilon \tag{4}$$

where SR is the set-recovery (%), β0 is the intercept, *f*1 and *f*2 are smooth functions (k = 3) for *CR* (compression ratio) and *D* (density), respectively; *ε* is the error term. In contrast, the TOLS regression, with a log-transformation applied to the set-recovery, provided insights into the potential multiplicative effects of compression ratio and density on set-recovery (Schmidt and Finan 2018). The TOLS is computed as:

$$\log(\mathrm{SR}) = \alpha 0 + \alpha 1 \times CR + \alpha 2 \times D + \epsilon \tag{5}$$

where SR is the set-recovery (%), α0 is the intercept, α1 and α2 are the coefficients for CR (compression ratio) and D (density), respectively; ε is the error term. Several diagnostic metrics such as Akaike Information Criterion (AIC), Bayesian Information Criterion (BIC), Mean Squared Error (MSE), Means Absolute Error (MAE), and Cross-validation (CV) error were performed to evaluate the performance of both models. These metrics were chosen for their capability to provide a comprehensive assessment of model fit and predictive accuracy (Cuny et al. 2013). The AIC is expressed as:

$$\mathrm{AIC} = 2k - 2\ln(L) \tag{6}$$

where *k* represents the number of parameters in the model, and ln(*L*) denotes the model's likelihood (Cuny et al. 2013). This metric is useful for model selection, where it balances

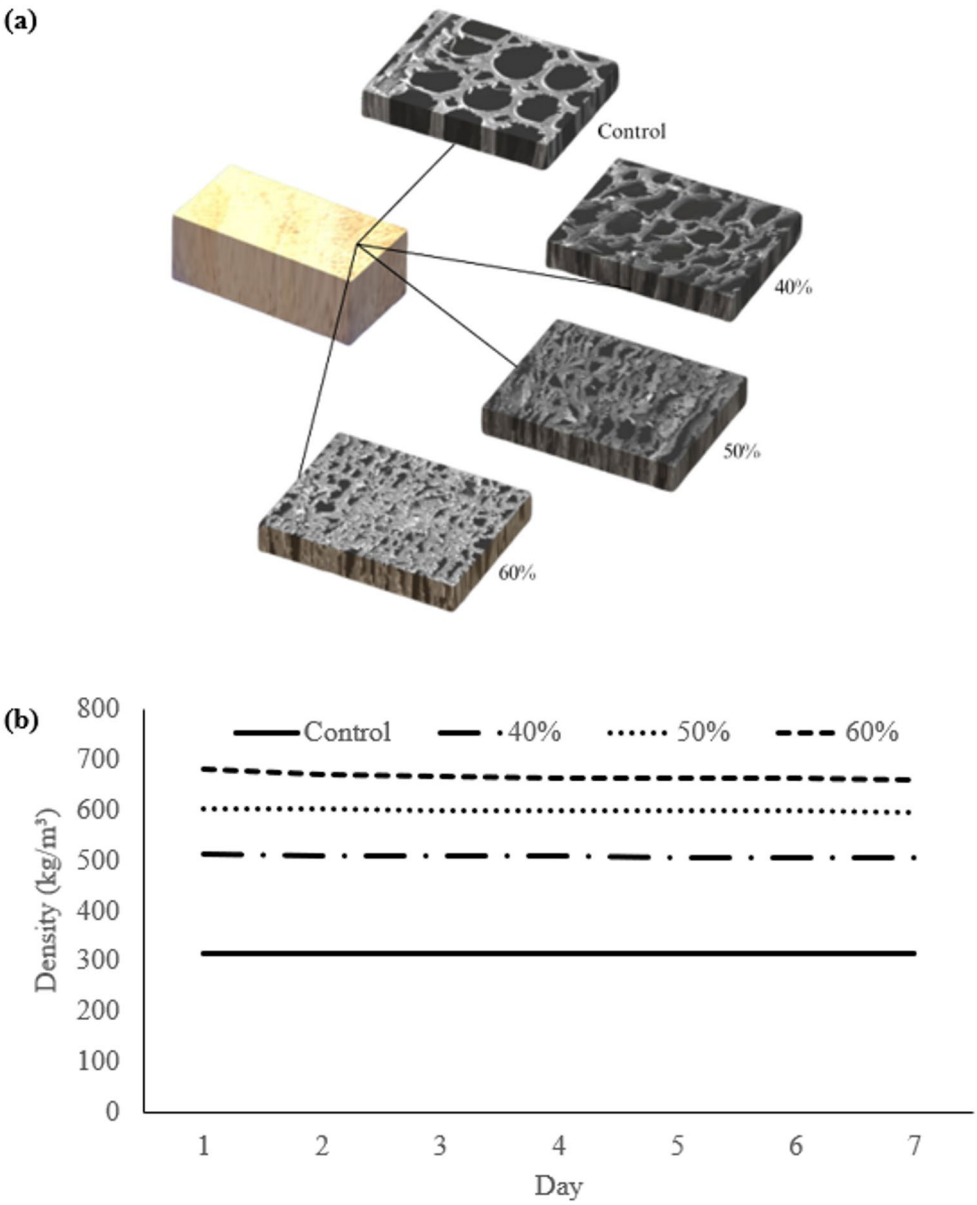


Fig. 7 Density: **a** the lumens of the densified laminas; **b** observation of density (mean values) over a seven-day period for the densified laminas

the model's complexity against its goodness of fit (Mermi et al. 2024). The BIC is calculated as:

$$\mathrm{BIC} = \ln(n)\,k - 2\ln(L) \tag{7}$$

where n is the number of observations, k is the number of parameters in the model, and ln(L) is the model's likelihood (Cagatay et al. 2016). Similar to AIC, BIC penalizes the number of parameters in the model, but generally applies more penalty for model complexity, especially for large n value (Mermi et al. 2024). The MSE is calculated as:

$$\mathrm{MSE} = \frac{1}{n}\sum_{i=1}^{n}(yi - \widehat{yi})^2 \tag{8}$$

where n is the number of observations, yi is the observed value, and $\check{y}i$ is the predicted value. MSE gives a measure of quality of an estimator, where the value is non-negative (Mermi et al. 2024). The MAE is calculated as:

$$\mathrm{MAE} = \frac{1}{n}\sum_{i=1}^{n}|yi - \widehat{yi}| \tag{9}$$

where n is the number of observations, yi is the observed value, and $\hat{y}i$ is the predicted value. Similar to MSE, MAE value is non-negative; however, it is more robust to outliers as it does not square the error terms (Schmidt and Finan 2018). CV error is computed as:

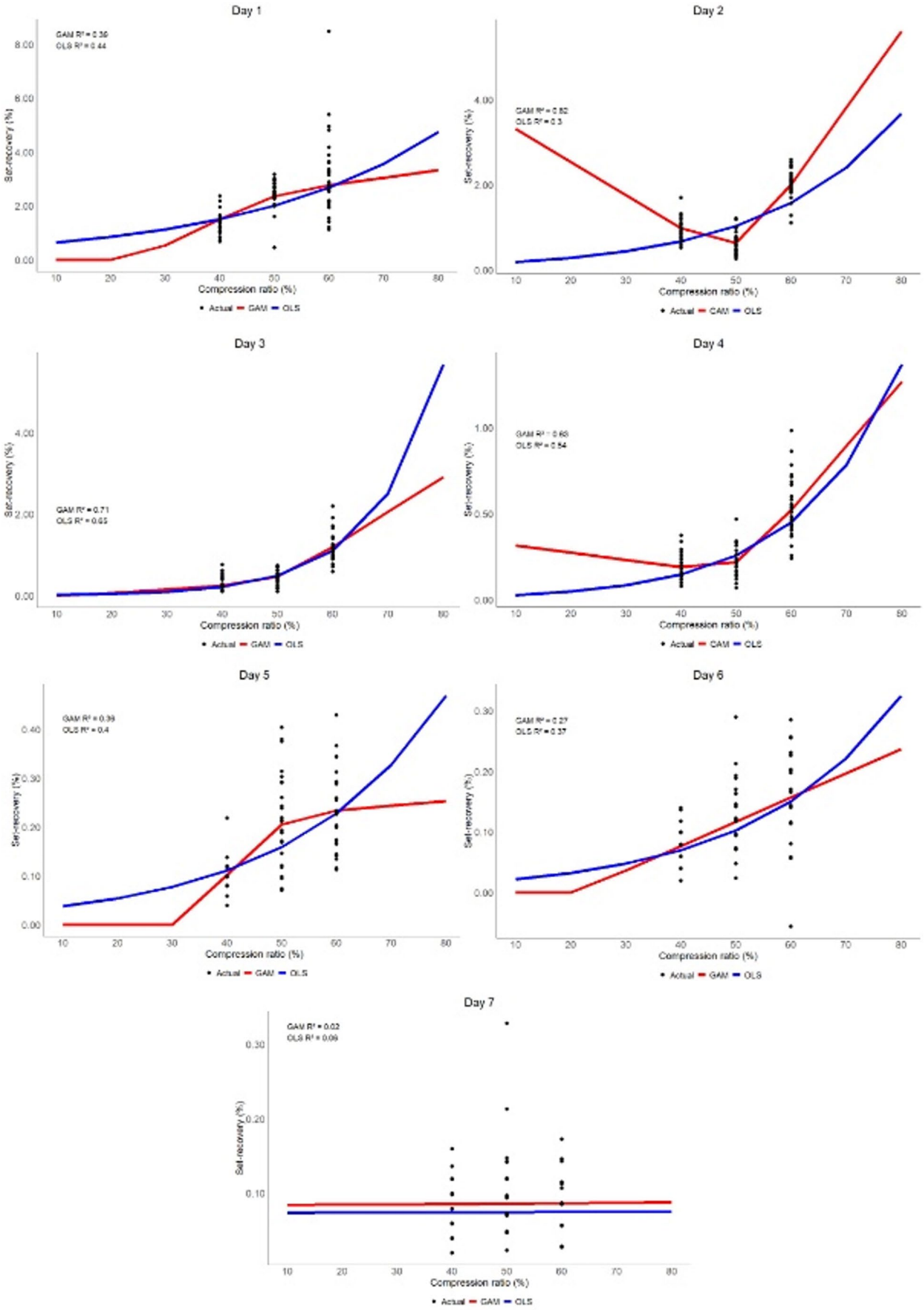

Day 1
GAM R² = 0.39
OLS R² = 0.44
Day 2
GAM R² = 0.82
OLS R² = 0.3
Day 3
GAM R² = 0.71
OLS R² = 0.65
Day 4
GAM R² = 0.68
OLS R² = 0.64
Day 5
GAM R² = 0.39
OLS R² = 0.4
Day 6
GAM R² = 0.27
OLS R² = 0.37
Day 7
GAM R² = 0.02
OLS R² = 0.09
Set-recovery (%)
Compression ratio (%)
Actual GAM OLS

Fig. 8 Comparison of GAM, TOLS, and actual data over seven days

$$\text{CV Error} = \frac{1}{k}\sum_{i=1}^{k} Ei \tag{10}$$

where k is the number of folds, Ei is the error metric (mean squared error) computed on the i-th fold. This metric provides a robust assessment by mitigating the potential bias introduced by a single train-test split (Cuny et al. 2013).

Result and discussions

Non-parametric tests

The results for the Kruskal-Wallis and Dunn tests were presented in Table 2, while the set-recovery and density observations were illustrated in Figs. 6 and 7, respectively.

During the first four days, the set-recovery for varying compression ratios showed notable fluctuations, which indicate the densified laminas' natural adaptive response to the compressive forces applied during the densification (Laine et al. 2014; Nilsson et al. 2014; Schwarzkopf 2021). It is possible that, during this period, the laminas undergo adjustment phase, where the internal structure of the wood cells reacts to the applied pressure, potentially involving microstructural reorientations and physicochemical transformations, suggesting a dynamic interaction between the lamina's structure and the external stresses, i.e., the relaxation of internal stresses (Fig. 6a), which led to a recovery in thickness aided by surrounding humidity (Neyses 2016; Darwis et al. 2017; Ran et al. 2023).

Subsequently, from the fifth day onwards, a notable shift towards stabilization in set-recovery rates was observed across all compression ratios, where this phase of stabilization indicates that the densified laminas achieved a state of equilibrium after a four-day adaptation phase (Fig. 6b). Although high compression ratios of up to 60% were applied, the laminas were able to achieve a stable set-recovery rate, which showed the capability of the densified laminas to attain an equilibrium state following a period of adaptation, highlighting their suitability for applications that require long-term stability and durability. From the first until the sixth day, there were significant differences between compression ratios of 40%, 50% and 60%. With chi-square values ranging from 30.69 to 66.58 and p-value <0.05, it was affirmed that compression ratio affected set-recovery. This trend, however, was slightly different on the seventh day, where no significant difference was found between the compression ratios. This outcome indicates the stabilization of the material, where the initial effect of compression or internal stress relaxation has equilibrated, and the densified laminas' set recovery is no longer affected by the compression ratios.

The density observation, on the other hand, exhibited a consistent pattern. From the first to the fourth day, the density of the densified laminas demonstrated a relatively stable trend, which might indicate the laminas' inherent structural rigidity (Fig. 7a-b) (Neyses et al. 2016a; Darwis et al. 2017). Unlike set-recovery, where internal adjustments and stress relaxation led to fluctuations, the density of the densified laminas was less influenced by such internal changes. This might be caused by the small percentage of set recovery or recovery in thickness, which did not significantly affect the volume and mass of the densified laminas (Buchelt et al. 2014; Neyses et al. 2016a; Schwarzkopf 2021).

From the fifth day onwards, this trend of consistent density continued without notable fluctuations, a key characteristic for applications where uniform and stable material properties are essential (Laine et al. 2016; Albert and Liew 2023). The consistent density across all compression ratios suggests that the densified laminas possessed a high degree of homogeneity and structural integrity, making them suitable for applications that demand predictable and stable material behaviour under stress (Albert and Liew 2023). Significant differences in density were observed across all compression ratios throughout the seven-day observation period. The chi-squared values remained high (43.40-49.23), and the p-values indicated strong statistical significance ($p<0.0001$). These results indicate that the level of compression remarkably influences density and remains consistent throughout time. Notably, the compression ratios appear to have a persistent and measurable effect on the material's density, an observation that may inform industrial applications where material density is a critical factor (Albert and Liew 2022a; Ran et al. 2023).

Comparative performance of models

In overall, GAM captured the relationship between set-recovery, density, and compression ratio better than TOLS. The prediction for each day was visualized in Fig. 8, while the goodness of fit for each model for the respective seven days was displayed in Table 3.

Based on the outcomes in Fig. 8, GAM captured the non-linear relationship between set-recovery, density, and compression ratios, while TOLS captured the linear relationship that showed an exponential trend. Despite the presence of outliers in the actual data points, both models still managed to capture the relationship accurately, and both approaches proved that set-recovery increased as the compression ratio increased. The model diagnostics (Table 3) indicated that GAM generated better predictions than TOLS because GAM captured lower values in all metrics. Lower AIC and

Table 3 Model diagnostics computed from the generalized additive model (GAM) and TOLS (Transformed ordinary least Square) regression

Day	AIC		BIC		MSE		MAE		CV	
	GAM	TOLS	GAM	TOLS	GAM	TOLS	GAM	TOLS	GAM	TOLS
1	-291.47	150.80	-281.47	160.80	0.98	0.96	0.64	0.68	0.002	0.002
2	34.99	134.58	47.48	144.58	0.10	0.33	0.24	0.49	0.087	0.435
3	9.57	120.42	21.96	130.41	0.07	0.07	0.19	0.18	0.070	0.072
4	-119.35	103.88	-106.94	113.88	0.02	0.02	0.10	0.10	0.023	0.022
5	-211.63	97.27	-199.47	107.27	0.01	0.01	0.06	0.06	0.007	0.007
6	-275.78	124.80	-265.82	134.76	0.003	0.003	0.04	0.04	0.003	0.003
7	-291.47	150.80	-281.47	160.80	0.002	0.04	0.002	0.03	0.002	0.002

BIC indicate better model fit, where these metrics penalize models' complexity, favouring more parsimonious models while balancing the goodness of fit (Cuny et al. 2013; Schmidt and Finan 2018; Mermi et al. 2024). As for MSE and MAE, lower values are indicative of higher prediction accuracy (Cuny et al. 2013). The difference between these two metrics is that MSE is sensitive to outliers, while MAE provides a more robust error measurement (Mermi et al. 2024). CV error, which is used in cross-validation, assesses the model's capability to generalize to new data (Schmidt and Finan 2018). A low CV error value is indicative of the model's accuracy in predicting unseen data, which enhances the model's reliability and usefulness in practical applications (Schmidt and Finan 2018).

During Days 1 (Fig. 8a) and 3 (Fig. 8c), both models have shown an increasing trend, where the 80% compression ratio obtained the maximum predicted set-recovery value of 5.68%. However, an irregular trend was captured by GAM on Day 2 (Fig. 8b), where 10% compression ratio was predicted to have a higher set-recovery than 50% compression. This prediction contradicted the hypothesis of the study: a higher compression ratio results in increased set-recovery. Nevertheless, this outcome did not reflect the overall pattern captured by the model.

During Day 4 (Fig. 8d), GAM also predicted that 10%, 20%, and 30% compression ratios would have higher set-recovery than 50% compression ratios; however, the predicted values were lower compared to the prediction on Day 2. From Day 5 until Day 7 (Fig. 8e-g), GAM predictions showed that 10% and 20% compression ratios had stable set-recovery, which indicated that the laminas had already attained an equilibrium state after the adaptation phase. TOLS, on the other hand, was more consistent throughout Days 1–6 (Fig. 8a-f), where the model captured an increasing trend. On Day 7 (Fig. 8g), both models predicted stable trends, indicating that the laminas had already stabilized and did not recover in thickness further.

The outcomes from both models have significant implications for the development of high-performance wood-based materials, where the accuracy of the predictions would assist researchers and practitioners in finding the balance between set-recovery and compression ratios, which would optimize the usage of low-density timber such as *Paraserianthes falcataria* in the industry.

Conclusions

The application of short-duration densification has resulted in the production of densified laminas of *Paraserianthes falcataria* with desirable properties. The outcomes from the non-parametric tests indicated that the compression ratio significantly influenced set recovery and density. Initially, set recovery shows variability, suggesting an adaptation phase, but it stabilizes over time. Density, in contrast, consistently aligns with the compression ratio, indicating a direct response to mechanical stress. Furthermore, the utilization of advanced modelling techniques, Generalized Additive Model (GAM) and Transformed Ordinary Least Square (TOLS) regression, provided a robust predictive trend. These models broadened our understanding of the densification process beyond the examined ratios, including a range of 10% to 80% compression ratios. It revealed GAM have higher prediction accuracy, given that it achieved lower model diagnostic metrics values than TOLS. Despite that, the outcomes from both models indicated that increasing compression ratios resulted in increasing set-recovery. These outcomes are critical for timber manufacturing, where understanding material behaviour under compression can lead to better-quality products. The novelty of this study was in applying a short-duration, three-phase densification process to a tropical fast-growing species (*Paraserianthes falcataria*), achieving stable densification under lower pressing temperature and reduced pressing time. This approach shortens the overall process while maintaining consistent material stability. Besides that, the study also contributes to the field by providing a clearer understanding of how compression ratio affects set-recovery and density, aiding in the development of more efficient and sustainable timber utilization strategies.

Acknowledgements The authors extend their gratitude to the Ministry of Higher Education (Malaysia), Universiti Malaysia Sabah, and the International Tropical Timber Organization (ITTO) for their financial support. This research was made possible through the Fundamental

Research Grant Scheme (FRGS/1/2022/TK10/UMS/02/1) and the ITTO Fellowship Programme (Reference No.: 070/21A).

Author contributions CMA: Conceptualization; Data curation; Formal analysis; Funding acquisition; Investigation; Methodology; Validation; Roles/Writing – original draft.KCL: Conceptualization; Funding acquisition; Project administration; Resources; Supervision; Visualization; Writing – review & editing.

Funding Open access funding provided by The Ministry of Higher Education Malaysia and Universiti Malaysia Sabah. The research was made possible by the funding from Ministry of Higher Education (Malaysia) (FRGS/1/2022/TK10/UMS/02/1) and the International Tropical Timber Organization (ITTO) (ITTO Fellowship Programme Reference No.: 070/21A).

Data availability No datasets were generated or analysed during the current study.

Declarations

Competing interests The authors declare no competing interests.

Open Access This article is licensed under a Creative Commons Attribution 4.0 International License, which permits use, sharing, adaptation, distribution and reproduction in any medium or format, as long as you give appropriate credit to the original author(s) and the source, provide a link to the Creative Commons licence, and indicate if changes were made. The images or other third party material in this article are included in the article's Creative Commons licence, unless indicated otherwise in a credit line to the material. If material is not included in the article's Creative Commons licence and your intended use is not permitted by statutory regulation or exceeds the permitted use, you will need to obtain permission directly from the copyright holder. To view a copy of this licence, visit http://creativecommons.org/licenses/by/4.0/.

References

Albert CM (2022) Properties of glue-laminated timber manufactured from viscoelastic-thermal compression modified Paraserianthes falcataria laminas. Master thesis, Universiti Malaysia Sabah

Albert CM, Liew KC (2022a) Effect of viscoelastic thermal compression (VTC) treatment on density and moisture content of laminas from paraserianthes falcataria. Adv Mater Process Technol 8:1–9. https://doi.org/10.1080/2374068X.2020.1799574

Albert CM, Liew KC (2022b) Influence of densification treatment on the morphology and density profile of paraserianthes falcataria laminas. Philipp J Sci 151:2509–2516. https://doi.org/10.56899/151.6B.15

Albert CM, Liew KC (2023) Recent development and challenges in enhancing fire performance on wood and wood-based composites: A 10-year review from 2012 to 2021. J Bioresour Bioprod 9:27–42. https://doi.org/10.1016/j.jobab.2023.10.004

Albert CM, Liew KC (2025) Influence of short-duration densification on the temperature profile of cross-laminated timber during an open burning test. J Korean Wood Sci Technol 53:119–128. https://doi.org/10.5658/WOOD.2025.53.2.119

Alinoori F, Moshiri F, Sharafi P, Samali B (2020) Reinforcement methods for compression perpendicular to grain in top/bottom plates of light timber frames. Constr Build Mater 231:116377. https://doi.org/10.1016/j.conbuildmat.2019.07.103

Bavaneghi F, Ghorbani M (2015) Mechanical behavior and springback of acetylated particleboard made in different press times. Wood Mater Sci Eng 11:57–61. https://doi.org/10.1080/17480272.2015.1006249

Bekhta P, Proszyk S, Krystofiak T et al (2015) Effects of short-term thermomechanical densification on the structure and properties of wood veneers. Wood Mater Sci Eng 1:40–54. https://doi.org/10.1080/17480272.2015.1009488

Buchelt B, Dietrich T, Wagenführ A (2014) Testing of set recovery of unmodified and furfurylated densified wood by means of water storage and alternating climate tests. Holzforschung 68:23–28. https://doi.org/10.1515/hf-2013-0049

Budakçı M, Pelit H, Sönmez A, Korkmaz M (2016) The effects of densification and heat post-treatment on hardness and morphological properties of wood materials. BioResources 11:7822–7838. https://doi.org/10.15376/biores.11.3.7822-7838

Cagatay B, Demir S, Aladag CH (2016) A comparison of different model selection criteria for forecasting EURO/USD exchange rates by feed forward neural network. Int J Comput Commun Instrum Eng 3:271–275. https://doi.org/10.15242/ijccie.u061610

Cuny HE, Rathgeber CBK, Kiessé TS et al (2013) Generalized additive models reveal the intrinsic complexity of wood formation dynamics. J Exp Bot 64:1983–1994. https://doi.org/10.1093/jxb/ert057

Darwis A, Wahyudi I, Dwianto W, Cahyono TD (2017) Densified wood anatomical structure and the effect of heat treatment on the recovery of set. J Indian Acad Wood Sci 14:24–31. https://doi.org/10.1007/s13196-017-0184-z

Fu Q, Cloutier A, Laghdir A (2017) Effects of heat and steam on the mechanical properties and dimensional stability of thermo-hygromechanically-densified sugar maple wood. BioResources 12:9212–9226. https://doi.org/10.15376/biores.12.4.9212-9226

Gonca Düzkale S, Ibrahim Bektas, Aysenur Kilic Ak (2019) Influence of combined heat treatment and densification on mechanical properties of Poplar wood. Maderas Ciencia Y tecnología 4:481–492. https://doi.org/10.4067/s0718-221x2019005000405

Kretschmann DE (2010) Mechanical properties of wood. In: Wood handbook—Wood as an engineering material. General Technical Report FPL-GTR-190. USDA Forest Service, Forest Products Laboratory, Madison, WI

Laine K, Segerholm K, Wålinder M et al (2014) Micromorphological studies of surface densified wood. J Mater Sci 49:2027–2034. https://doi.org/10.1007/s10853-013-7890-8

Laine K, Segerholm K, Wålinder M et al (2016) Wood densification and thermal modification: hardness, set-recovery and micromorphology. Wood Sci Technol 50:883–894. https://doi.org/10.1007/s00226-016-0835-z

Luan Y, Fang CH, Ma YF, Fei BH (2022) Wood mechanical densification: a review on processing. Mater Manuf Process 37:359–371. https://doi.org/10.1080/10426914.2020.1856134

Mermi S, Akkuş Ö, Göktaş A, Gündüz N (2024) A new robust ridge parameter estimator having no outlier and ensuring normality for linear regression model. J Radiat Res Appl Sci 17:100788. https://doi.org/10.1016/j.jrras.2023.100788

Navi P, Heger F (2004) Combined densification and thermo-hydro-mecahnical processing of wood. Wood Sci Technol 37:151–164

Neyses B (2016) Surface-densified wood: from laboratory-scale research towards a competitive product. Eur J Wood Wood Prod 13:19–19

Neyses B, Hagman O, Sandberg D, Nilsson A (2016a) Development of a continuous wood surface densification process: The roller pressing technique. In: Proceedings of the International Convention of Society of Wood Science and Technology: Forest Resource and Products: Moving Toward a Sustainable Future, Monona, United States, pp 17–24

Neyses B, Rautkari L, Yamamoto A, Sandberg D (2016b) Reduction of the set-recovery of surface-densified scots pine by pre-treatment with sodium silicate or sodium hydroxide. In: Proceedings of COST Action FP1407 2nd Conference – Innovative production technologies and increased wood products recycling and reuse, Brno, Czech Republic, pp 57–58

Nilsson J, Johansson J, Sandberg D (2014) Densified and thermally modified wood in light-weight panels. In: Proceedings of the Forest Products Society International Convention, Quebec City, Canada, pp 1–6

Pelit H, Budakçı M, Sönmez A et al (2018) Density and some mechanical properties of densified and heat post-treated Uludağ fir, Linden and black Poplar woods. Eur J Wood Wood Prod 76:79–87. https://doi.org/10.1007/s00107-017-1182-y

Ran Y, Lu D, Jiang J et al (2023) Deep eutectic solvents-assisted wood densification: a promising strategy for shape-fixation. Chem Eng J 471:144476. https://doi.org/10.1016/j.cej.2023.144476

Schmidt AF, Finan C (2018) Linear regression and the normality assumption. J Clin Epidemiol 98:146–151. https://doi.org/10.1016/j.jclinepi.2017.12.006

Schwarzkopf M (2021) Densified wood impregnated with phenol resin for reduced set-recovery. Wood Mater Sci Eng 16:35–41. https://doi.org/10.1080/17480272.2020.1729236

Schwarzkopf M, Burnard M, Pastur GM et al (2018) Performance of three-layer composites with densified surface layers of *Nothofagus pumilio* and *N. antarctica* from Southern Patagonian forests. Eur J Wood Wood Prod 0272. https://doi.org/10.1080/17480272.2017.1366945

Srivaro S, Lim H, Li M et al (2021) Effect of compression ratio and original wood density on pressing characteristics and physical and mechanical properties of thermally compressed coconut wood. Constr Build Mater 299:124272. https://doi.org/10.1016/j.conbuildmat.2021.124272

Tu D, Su X, Zhang T et al (2014) Thermo-mechanical densification of *Populus tomentosa* var. *tomentosa* with low moisture content. BioResources 9:3846–3856. https://doi.org/10.15376/biores.9.3.3846-3856

Wang Z, Gao Y, Zhou Y et al (2023) Pyrolysis and combustion behaviors of densified wood. Proc Combust Inst 39:4175–4184. https://doi.org/10.1016/j.proci.2022.08.057

Zhan J, Avramidis S (2018) Needle Fir wood modified by surface densification and thermal post-treatment: hygroscopicity and swelling behavior. Eur J Wood Wood Prod 74:49–56. https://doi.org/10.1007/s00107-015-0969-y

Zhao Y, Wang Z, Iida I et al (2015) Studies on pre-treatment by compression for wood drying I: effects of compression ratio, compression direction and compression speed on the reduction of moisture content in wood. J Wood Sci 61:113–119. https://doi.org/10.1007/s10086-014-1451-x

Publisher's note Springer Nature remains neutral with regard to jurisdictional claims in published maps and institutional affiliations.